Nanoporous Polycyanurates Created by Chemically-Induced Phase Separation: Structure-Property Relationships

Olga Grigoryeva,*[1] *Alexander Fainleib*,[1] *Kristina Gusakova*,[1] *Olga Starostenko*,[1] *Jean-Marc Saiter*,[2] *Volodymyr Levchenko*,[1,3] *Anatoli Serghei*,[3] *Gisèle Boiteux*,[3] *Daniel Grande*[4]

Summary: Nanoporous thermostable polycyanurate (PCN) films were generated by *in-situ* metal complex-catalyzed polycyclotrimerization of 4,4′-ethylidenediphenyl dicyanate in the presence of 20–50 wt.% of inert high-boiling temperature liquids as porogens, *i.e.* dioctyl, dibutyl or dimethyl phthalates (DOP, DBP or DMP), followed by their extraction from the densely crosslinked PCN frameworks, drying, and additional annealing at various temperatures. The nanoporous structure for all PCN-based films developed was investigated by SEM, BET, and DSC-based thermoporometry. Furthermore, the thermal and dielectric properties of the nanoporous films were also examined. The method developed allows producing nanoporous films for membranes with controlled thermal and dielectric properties as well as porosity parameters.

Keywords: chemically-induced phase separation; nanoporous thermosets; polycyanurate network; structure-property relationships; thermal annealing

Introduction

Polycyanurates (PCNs) represent a family of high-performance thermosetting polymers with excellent dimensional and chemical stability, inherent flame-retardancy, high-glass transition temperatures ($T_g \sim$ 220–270 °C), low dielectric constants ($\varepsilon \sim$ 2.6–3.2), and high adhesion to conductor metals and glass fiber, carbon fiber etc.[1–3] PCNs obtained by polycyclotrimerization of Cyanate Ester Resins (CER) can be useful for producing porous or nanoporous films, which have a wide array of applications as thermostable membranes, filters, sensors, or sorbents in filtration, separation and depuration processes.[4–6]

Recently, different series of nanoporous PCN-based film materials were developed by some of us using the chemically-induced phase separation approach.[7] Hydrolytically labile poly(ε-caprolactone) (PCL) oligomers[8,9] or chemically inert high-boiling temperature plasticizers,[10,11] such as dimethyl phthalate (DMP) or dibutyl phthalate (DBP), were used as porogen agents.

The aim of the present work consists in synthesizing high-crosslink density PCNs in the presence of a highly effective and selective catalytic complex, and then in creating thermostable nanoporous films by chemically-induced phase separation using varying contents (20–50 wt.%) of different inert high boiling temperature plasticizers as porogens. Furthermore, we shall investigate

[1] Institute of Macromolecular Chemistry, National Academy of Sciences of Ukraine, Kharkivske shose 48, 02160 Kyiv, Ukraine
E-mail: grigoryevaolga@i.ua
[2] AMME-LECAP International Lab. Institute for Material Research, Université de Rouen, Faculté des sciences, BP12, 76801 Saint Etienne du Rouvray, France
[3] Université de Lyon, Université Lyon1, CNRS-UMR 5223 Ingénierie des Matériaux Polymères, 69622 Villeurbanne, France
[4] Institut de Chimie et des Matériaux Paris-Est, UMR 7182 CNRS – Université Paris-Est Créteil Val-de-Marne, 94320 Thiais, France

the influence of additional annealing, needful to completely remove the porogens from the densely crosslinked PCNs, on chemical structure and porous morphology, as well as the thermal and dielectric properties of the nanoporous PCN-based films developed.

Experimental Part

Materials

4,4′-Ethylidenediphenyl dicyanate (dicyanate ester of bisphenol E, DCBE), under the trade name Primaset LECy, was kindly supplied by Lonza (Lonza, Switzerland). A mixture of cobalt acetyl acetonate (100 ppm) and nonylphenol (2 phr) was used as a catalytic complex; these compounds were supplied by Sigma-Aldrich. High-boiling porogens, such as dioctyl phthalate (DOP, $\geq$ 99.5%, b.p. ~384 °C, M ~ 309.6 g•mol^{-1}, $T_m \approx -55$ °C), dibutyl phthalate (DBP, $\geq$ 99%, b.p. ~ 340 °C, M ~ 278.3 g • mol^{-1}, $T_m \approx -35$ °C) or dimethyl phthalate (DMP, purity $\geq$ 99%, b.p. ~ 282 °C, M ~ 194.2 g • mol^{-1}, $T_m \approx$ 0–2 °C) were supplied by Sigma-Aldrich. All the chemicals were used as received.

Preparation of PCN-Based Films

DCBE was mixed with DOP (DBP or DMP) in a given ratio (the content of phthalates was varied from 20 to 50 wt.%), and then poured into a PTFE-coated mold and heated through the following step-by-step schedule: 150 °C for 5 h, then 180 °C for 3 h, and finally 210 °C for 1 h. Unlike our previous report,[10] to accelerate the polycyclotrimerization of DCBE, to shift the reaction temperature interval to lower temperatures and to minimize the dilution effect of liquid phthalates, a catalytic metal complex was used.[12,13] It is noteworthy that some limitation in the formation of PCN-based films in the presence of phthalates due to a dilution effect was found experimentally, and the critical content of the DOP, DBP, and DMP in the initial mixture with DCBE was determined: it was equal to 20 wt.% for DOP, 30 wt.% for DBP, and 50 wt.% for DMP. The following codes were applied to the samples studied: PCN_{DOP20}, PCN_{DBP30}, PCN_{DMP30}, PCN_{DMP50}, where the subscripts indicate the type and the initial content of the porogen used. The films obtained with a thickness around 300 μm were subjected to extraction with acetone in a Soxhlet apparatus for 24 h. During extraction of the phthalates followed by drying of the samples up to a constant weight at 50 °C, a porous structure in the PCN-based films was generated. Afterwards, in order to reach complete removal of non-extracted porogens from densely crosslinked PCN matrices, an additional annealing of the samples at different temperatures (T ~ 50, 100 or 150 °C for 48 h, as well as at T ~ 250 °C for 2 h or 24 h) was performed.

Characterization Techniques

The morphology of the samples was examined by Scanning Electron Microscopy (SEM) using a LEO 1530 microscope equipped with a high-vacuum Gemini column. Prior to analyses, the samples were cryo-fractured and coated with a Pd/Au alloy in a Cressington 208 HR sputter-coater. Pore sizes and pore size distribution were determined using the Image J 1.45s software.

DMTA was carried out with a TA Instruments Q800 thermal analyzer in bending mode. Rectangular samples were cut from films within the following range of dimensions: length of 40 mm, width of 5 mm, and thickness of 0.5 mm. Storage modulus (E') and loss factor (tan δ) were measured between −50 and 320 °C at a heating rate of 3 °C/min and a frequency of 10 Hz. Two heating runs were performed.

Thermogravimetry analysis (TGA) was performed on a Netzsch TG 209 thermobalance under nitrogen atmosphere. Sample pellets with masses ranging from 10 to 20 mg were heated at 20 °C · min^{-1} from 20 °C up to 700 °C.

Differential Scanning Calorimetry (DSC) measurements were performed with a TA Instruments Q100 calorimeter under nitrogen atmosphere. For DSC-based thermoporometry measurements, the scans were

run from −50 to 5 °C at a heating rate of 1 °C · min^{-1}. To increase the hydrophilicity of the porous PCNs and facilitate the penetration of water into their pores, the samples were first immersed in ethanol overnight. After this preliminary treatment, deionized water was gradually added to remove the ethanol.[14,15] The samples were placed for 1 h in ethanol/water mixtures of different volume compositions (90/10, 70/30, 50/50, and 30/70 vol.%), and they were then immersed in pure water for 2 weeks. From melting thermograms of water, the melting temperature (T_m) depression due to water contained inside the pores of polycyanurate network were correlated to the pore diameter D_p as indicated by Eq. (1):[14,15]

$$D_p(nm) = 2 \cdot \left(0.68 - \frac{32.33}{T_m - T_{m0}}\right), \qquad (1)$$

where T_m and T_{m0} are the melting temperatures of confined and bulk water, respectively. The pore size distribution dV_p/dR_p *vs.* D_p was derived from the melting thermograms by using Eq. (2):[14,15]

$$dV_p/dR_p(cm^3 \cdot nm^{-1} \cdot g^{-1}) = \frac{dq/dt \cdot (T_m - T_{m0})^2}{32.33 \cdot \rho \cdot v \cdot m \cdot \Delta H(T)}, \qquad (2)$$

where dq/dt stands for the heat flow recovered by DSC; ρ, v, m are the water density, the heating rate, the sample mass, respectively. The melting enthalpy of water crystallites $\Delta H(T)$ was determined by using Eq. (3):[14,15]

$$\Delta H(T)(J \cdot g^{-1}) = 332 + 11.39 \cdot (T_m - T_{mo}) + 0.155 \cdot (T_m - T_{m0})^2 \qquad (3)$$

Nitrogen sorption measurements were carried out at −196 °C with a Micromeritics ASAP 2010 porosimeter. The specific surface area values for the investigated porous polymers were quantified using the Brunauer, Emmett and Teller (BET) method at relative pressure (P/P_0) values ranging from 0.05 to 0.3.

Dielectric measurements were performed using a Novocontrol high resolution alfa dielectric analyzer in the frequency range of 10^{-1}–10^{7} Hz. The samples were examined using circular brass plates of 20 mm diameter as electrodes. The thickness of the samples was uniform (about 0.3 mm). The applied voltage was 0.5 V and the experiments were carried out at room temperature. Before any measurement, all the samples were vacuum-dried during 6 h at 30 °C.

Results and Discussion

Generation of Porous Frameworks and Morphology Characterization

The SEM investigation (Figure 1) confirmed the generation of nanoporous structure in the PCN-based films after extraction of DOP, DBP or DMP, the sizes (pore diameters, D_p) of spherical pores being found in the range between $D_p \sim 13$ and 230 nm (see Table 1). The highest content of spherical pores of large diameter ($D_p > 100$ nm) was observed for the PCN_{DOP20} sample (Figure 1a). Even the PCN_{DPM50} sample (Figure 1b), containing a higher amount of porogen in the initial system, displayed a lower content of large pores even though its total pore volume was higher, as it will be shown by DSC-based thermoporometry (Table 1).

For all PCN-based samples after their annealing at different temperatures, the presence of pores was also observed (Figure 2). Finally, one could conclude that no significant collapse of pores occurred, even for the highest annealing temperature applied, *i.e.* 250 °C (Figure 2 c,d). In a previous study from Hedrick *et al.*,[16] the collapse of pores was observed after additional thermal treatment of porous samples based on PCNs modified by poly(oxypropylene).

Note, in order to generate pores in the samples studied by the chemically-induced phase separation technique, the porogen should stay within the network up to the final stage of curing, *i.e.* 210 °C, and then has to be extracted from the resulting network. Therefore, the porogen should possess a higher boiling temperature than that of the

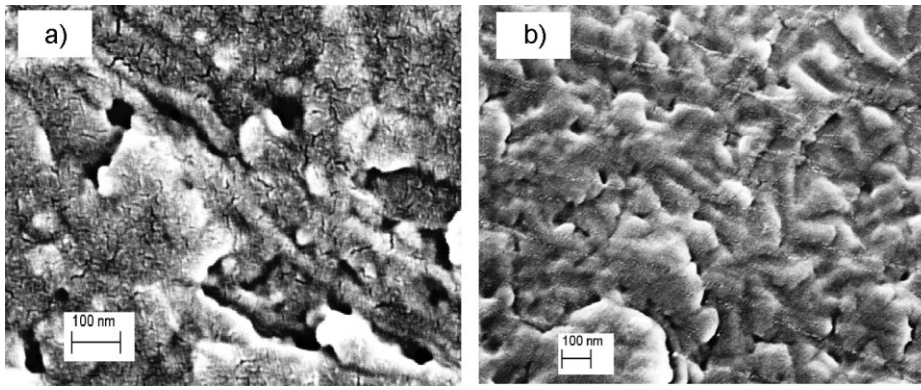

Figure 1.
SEM micrographs of nanoporous PCN-based films created by porogen extraction: (a) 20 wt.% DOP; (b) 50 wt.% DMP.

last step of PCN curing and be inert towards cyanate ester resins to prevent chemical grafting onto the network. Certainly, a two-phase morphology structure is generated during the curing process as the forming PCN framework is immiscible with the phthalate porogen. Furthermore, to evaluate the miscibility of DCBE with the high-boiling temperature phthalates, their Hildebrand's solubility parameters (δ) were compared: $\delta_{DOP} = 16.8$ MPa$^{1/2}$; $\delta_{DBP} = 19.0$ MPa$^{1/2}$;$\delta_{DMP} = 21.9$ MPa$^{1/2}$; $\delta_{DCBE} = 22.1$ MPa$^{1/2}$.[17] One can suppose that the higher the difference between solubility parameter values of DCBE and the phthalate chosen, the higher the degree of phase separation[18] occurring in the resulting PCN/phthalates samples, which should result in an increase in the average size of pores formed after porogen extraction. Moreover, one can suppose that the difference in the critical concentrations of different phthalates used for affording PCN-based films, as discussed above in the Experimental part, is also due to the differences in the solubility parameters.

Structure Characterization of PCN-Based Films

The chemical structures of precursory PCN/porogen and resulting porous PCN-based films were shown and confirmed by FTIR

Table 1.
Main porosity characteristics for nanoporous PCN-based films after phthalate extraction followed by their annealing at different temperatures.

Sample code	Temperature of annealing (°C)	Pore size distribution, D_p (nm)		Average pore diameter, $D_{p(av)}$[a] (nm)	Total pore volume, V_p[a] (cm$^3 \cdot$ g^{-1})
		SEM	DSC		
PCN_{DOP20}	–	17–155	15–170	33	0.08
	50	13–150	15–155	45	0.13
	150	14–145	20–150	65	0.14
PCN_{DBP30}	—	20–150	15–160	49	0.12
	50	15–145	15–130	45	0.11
	150	25–140	20–130	36	0.16
PCN_{DMP30}	—	17–170	15–180	33	0.19
	50	14–190	10–200	23	0.22
	150	20–195	15–220	29	0.31
PCN_{DMP50}	—	15–190	20–185	34	0.34
	50	20–200	15–195	35	0.29
	150	18–210	15–230	43	0.35

[a] values as determined by DSC-based thermoporometry.

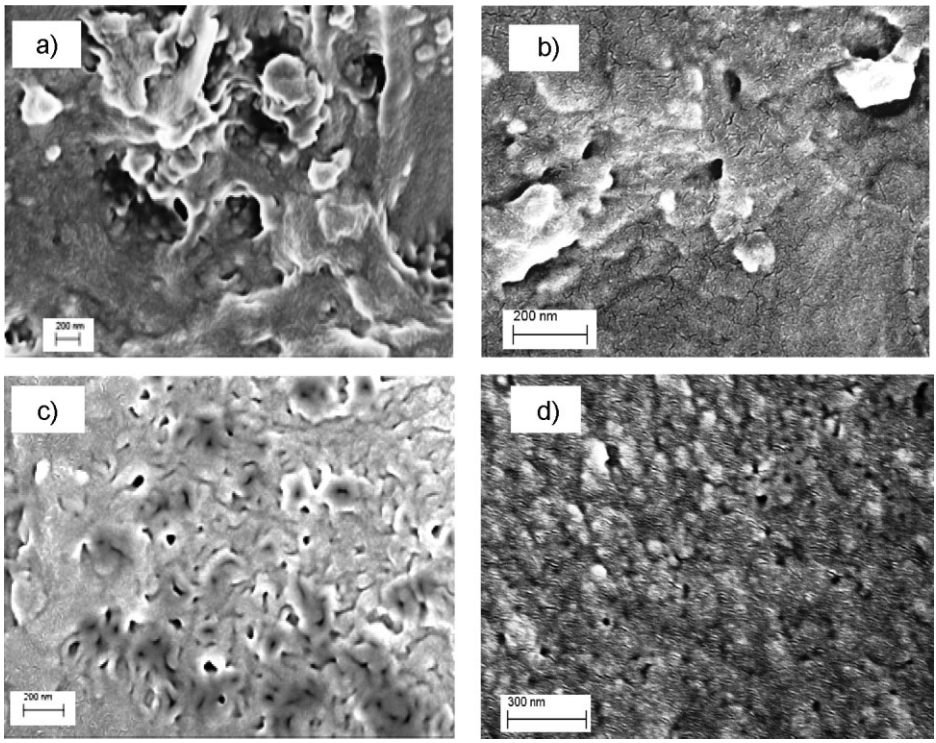

Figure 2.
Typical SEM micrographs of nanoporous PCN-based samples created by porogen extraction followed by their annealing at different temperatures: (a) PCN_{DOP20}, 100 °C, 48 h; (b) PCN_{DBP30}, 100 °C, 48 h; (c) PCN_{DMP30}, 250 °C, 24 h; (d) PCN_{DMP50}, 250 °C, 24 h.

analysis elsewhere.[10,11] Briefly, the appearance of —C=N— and phenylene–oxygen–carbon valence vibrations (at 1358 cm^{-1} and 1557 cm^{-1}, respectively) in triazine cycles of PCNs and the absence of cyanate groups of DCBE were established. The presence of phthalates in the PCN matrix directly after the synthesis of the samples and the porogen removal from the PCN networks after extraction of phthalates by acetone were confirmed also by FTIR and gel fraction content data.[10,11] However, the presence of ~7 wt.% of residual phthalates in PCN_{DOP20} and PCN_{DMP50} samples was found after the extraction procedure.[11] It was found that the porous PCN samples after their thermal annealing did not contain any residual porogen. However, some changes in the chemical structure of porous PCN samples annealed at the temperature of 250 °C for 24 h were detected by FTIR,[11] which could be ascribed to the partial thermally-induced degradation of cyanurate cycles of PCNs accompanied by release of amines, phenols, and derivatives of cyanuric acid.[19,20]

The phthalates used are well-known plasticizers [21] which could affect the glass transition behavior and the thermal stability of the samples studied. Three samples were then investigated by DMTA (Figure 3) and TGA (Figure 4) to check the effect of DMP on their viscous-elastic properties (*i.e.* glass transition temperature, T_g) and thermal stability (*i.e.* temperature of thermal degradation, T_d).

The DMTA investigation carried out for the initial PCN/DMP 50/50 wt.% sample (before extraction of porogen) confirmed a significant decrease in the glass transition

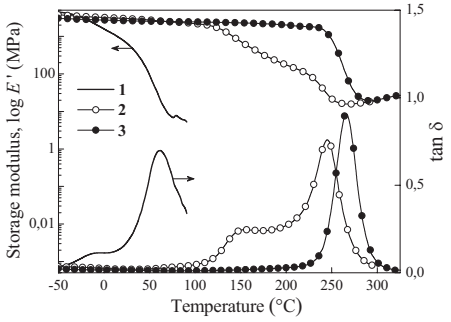

Figure 3.
Temperature dependence of storage modulus (E') and tangent delta (tan δ) for the samples studied: (1) initial PCN/DMP 50/50 wt.% (*i.e.* before extraction of porogen); (2) nanoporous PCN_{DMP50}, 1st heating run; (3) nanoporous PCN_{DMP50}, 2nd heating run.

temperature value of PCN matrix ($T_g \approx 61\,^{\circ}C$, Figure 3, curve 1), due to the presence of a high amount of DMP. For the extracted PCN_{DMP50} sample, two glass transition regions with $T_{g1} \approx 151\,^{\circ}C$ and $T_{g2} \approx 245\,^{\circ}C$ as well as the corresponding two step-drop mechanism in the storage modulus ($log\ E' = f(T)$) were observed (Figure 3, curve 2). The presence of the two T_g's can be explained by the occurrence of a microphase-separated morphology with domains containing both PCN and residual DMP (T_{g1}), and a pure PCN microphase (phthalate-free) with a higher T_{g2} value. For the extracted PCN_{DMP50} sample after the second heating DMTA run, only one T_g value was observed ($T_g \approx 266\,^{\circ}C$, Figure 3, curve 3), which evidenced the absence of the plasticizer in the sample. One could conclude that in such a sample, DMP was completely evaporated from the PCN matrix.

The above conclusions were in a good agreement with the corresponding TGA data (Figure 4). For the initial PCN/DMP 50/50 wt.% sample (before extraction of porogen), a significant mass loss ($\sim$ 49 wt.%) in a temperature range T_{d1} varying from $\sim 160\,^{\circ}C$ to $430\,^{\circ}C$ (Figure 4, curve 1) occurred, due to the evaporation of DMP. The thermal degradation of the PCN network started at $T_{d2} \approx 441\,^{\circ}C$. For the extracted PCN_{DMP50} sample, only $\sim$7 wt.% of mass loss occurred in a temperature range T_{d1} ranging from $100\,^{\circ}C$ to $305\,^{\circ}C$ (Figure 4, curve 2), due to the evaporation of bulk and confined water and residual porogen.

The thermal degradation of PCN started at $T_{d2} \approx 442\,^{\circ}C$. For the PCN_{DMP50} sample after 1st heating run by DMTA, no additional mass loss was observed (Figure 4, curve 3) before the thermal degradation of PCN at $T_d \approx 440\,^{\circ}C$, which evidenced the absence of any residual porogen in the sample.

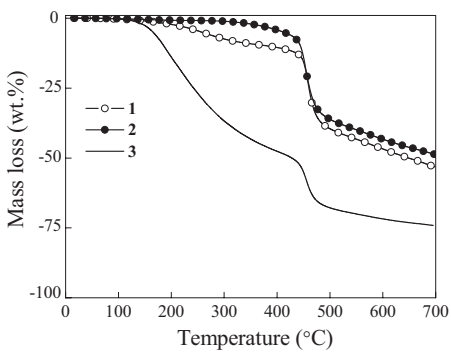

Figure 4.
TGA curves for the samples studied: (1) initial PCN/DMP 50/50 wt.%; (2) nanoporous PCN_{DMP50}; (3) nanoporous PCN_{DMP50} after 1st heating run by DMTA.

Effect of Thermal Annealing on Thermal Properties of Nanoporous PCN-Based Films

The effect of thermal annealing in air on mass loss values for PCN_{DOP20}, PCN_{DBP30}, PCN_{DMP30} and PCN_{DMP50} samples was investigated, and a well-defined effect of annealing temperature and time on sample mass loss was found (plots not shown here). It was concluded that the higher the temperature and the longer the time, the higher the sample mass loss value [11]. For the samples annealed at $T \approx 50$–$150\,^{\circ}C$ for 48 h, it was found that constant masses could be reached after an annealing time of $\tau \sim 5$ h. The maximal mass loss was fixed to be equal to around 2–7 wt.% depending on the sample studied, which could be attributable to the evaporation of some water traces and/or residual porogen. However, for the samples annealed at $T \approx 250\,^{\circ}C$ after

$\tau \sim 5$ h, the mass loss was around 15–17 wt. %. No constant mass was reached even after $\tau \sim 24$ h of heating time, while a darkening and an increasing brittleness of the samples were observed. This could be explained by the aforementioned partial thermal-oxidative degradation of PCN structures.[19,20]

The thermal stability (in N_2) of initial nanoporous samples (after porogen extraction only) and the extracted samples after annealing at different temperatures were studied by TGA; typical TGA curves are shown in Figure 5. For each nanoporous PCN sample, one could observe three main degradation stages. The first stage for a temperature up to $T \sim 200\,^{\circ}C$ corresponded mainly to the evaporation of bulk and confined water; the mass loss value (Δm) for all the samples was equal to around 1.1–3.6 wt.%. The second stage of degradation in a temperature range of $T \sim 300$–$440\,^{\circ}C$ was caused by the destruction of fragments in the PCN network with low crosslink density. Finally, the third stage for temperatures higher than $T \sim 450\,^{\circ}C$ could be attributed to the destruction of the molecular skeleton of PCN.[19,20]

In Figure 5a, one could see some differences in thermal stability for the nanoporous PCN-based samples created by using different phthalates as porogens: the higher thermal stability was observed for PCN_{DOP20} and PCN_{DMP30} samples. However, thermal annealing of the samples resulted in the disappearance of these differences (Figure 5b as typical examples): obviously enough, a similar post-curing process occurred in all the samples during annealing. It was also found that the higher the annealing temperature of the samples, the higher their thermal stability, which suggested an increasing crosslink density of the PCN network as a result of post-curing. However, for all the nanoporous PCN-based samples annealed at $T = 250\,^{\circ}C$, some decrease in the thermal stability was observed (data not shown here). One could conclude that long-term annealing at such a high temperature was accompanied by the aforementioned partial thermal degradation of the network skeleton. Nevertheless, all the nanoporous PCN-based films studied could be considered as highly thermostable materials.

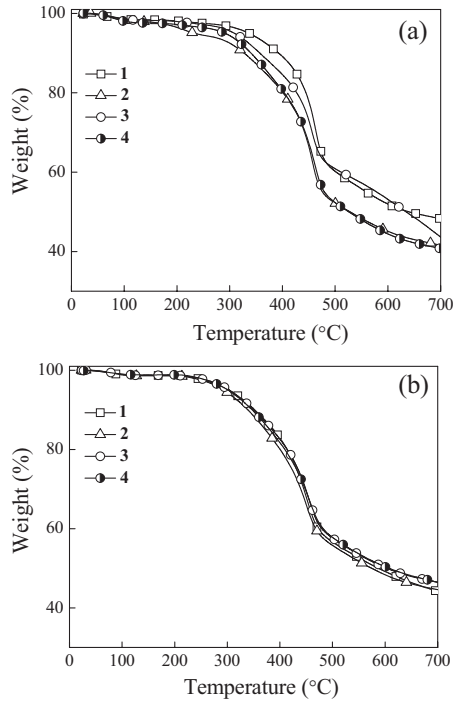

Figure 5.
Typical TGA curves for nanoporous PCN-based films: (a) samples after porogen extraction only; (b) samples after porogen extraction followed by annealing at $T = 150\,^{\circ}C$; (1) PCN_{DOP20}; (2) PCN_{DBP30}; (3) PCN_{DMP30}; (4) PCN_{DMP50}.

Porosity Features of Nanoporous PCN-Based Films

Additional information on the nanoporous structure generated in the PCN samples after extraction of the phthalates as well as those after thermal annealing was provided by DSC-based thermoporometry and BET analyses. In Figure 6, the melting thermograms of water in the temperature region between $-5\,^{\circ}C$ and $5\,^{\circ}C$ (Figure 6a) and the corresponding profiles of pore size distributions (Figure 6b) are given for nanoporous PCN_{DBP30} samples of different annealing temperatures. In the thermograms of PCN_{DBP30} samples, two

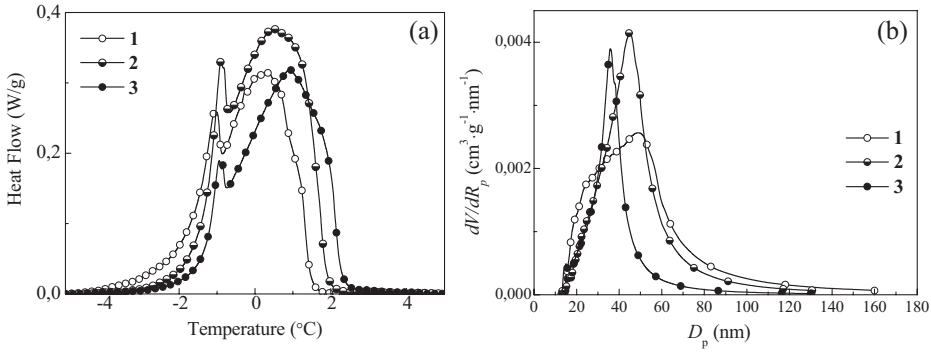

Figure 6.
(a) Typical DSC melting thermograms of water and (b) corresponding pore size distribution profiles as determined by DSC-based thermoporometry for nanoporous PCN_{DBP30} samples: (1) after extraction of porogen; after additional annealing at (2) $T = 50\,^{\circ}C$ or (3) $T = 150\,^{\circ}C$.

endothermic peaks were detected, namely one corresponding to the melting of water constrained within the pores of the films (Tm), and a second one related to the melting of bulk water with a maximum around 0–1 °C (Tm0, Figure 6a). Similar thermograms were obtained for all other PCN-based samples studied (data not shown here). It was found that the intensity of the melting peaks strongly depended on the initial phthalate content: a higher porogen content was associated with an increase in the peak intensity due to the melting of a higher volume of confined water. Therefore, an increase in the phthalate content resulted in an increase in the peak intensity of dV/dR_p *vs.* Dp curves, thus providing a higher total pore volume (V_p) and, in general, increasing the annealing temperature of the samples also resulted in increasing V_p values, as expected (Table 1). Even though pore size distributions of the PCN-based films studied were in the range of ~15–230 nm, their average pore diameters were centered around ~23–65 nm (Table 1). It should be noted that pore diameters smaller than 50 nm represented up to ~80–90% of all the pore sizes. It is also noteworthy that the data determined using DSC-based thermoporometry matched quite well the results obtained by SEM analysis (see Figures 1,2 and Table 1).

The specific surface area (S_p) is one of the most important features in the characterization of porous materials, and BET analysis is the standard method for its determination from nitrogen adsorption isotherms [22]. When the BET method was applied to some nanoporous PCN-based samples studied, it was found that thermal annealing generally increased their S_p values, as expected, due to an increase in their V_p values. For example, for the nanoporous PCN_{DMP30} sample, the S_p value was equal to around 30 m^2/g, while for the PCN_{DMP30} sample after annealing at $T = 150\,^{\circ}C$, the S_p value increased up to 70 m^2/g.

Similarly, for the nanoporous PCN_{DBP30} sample before any annealing, the S_p value was equal to 61 m^2/g, and after annealing at $T = 150\,^{\circ}C$, the S_p value increased up to 167 m^2/g. Accordingly, such results were in accordance with the conclusions inferred from the DSC-based thermoporometry and SEM data.

Dielectric Measurements of PCN-Based Films

The study of the relevant conditions of dielectric measurements was first performed, and the preparation of the films was carefully proceeded to get a regular thickness and flat surface in order to decrease as much as possible the errors of the determination of

the permittivity values. The variations of the permittivity versus frequency had similar shapes, namely smoothly constant in the whole frequency domain, as shown in Figure 7, indicating that no Maxwell-Wagner-Sillars effects or interfacial polarizations are observed [23]. This indicates that there was no significant heterogeneity content in the samples studied, as this would have resulted from the pore formation in the case that a difference in the conductivity of the two phases would exist.

The neat PCN film presented a permittivity ε' at 1 KHz equal to 3.29 (Figure 7, curve 1), which was relatively low and is known for polycyanurates [1]. It is noteworthy that the neat PCN sample was extracted in the same conditions as those used for the other samples. In the case of PCN_{DBP30} (Figure 7, curve 2, at 1 kHz, $\varepsilon' \sim 3.31$), the values of ε' were slightly higher than those for the neat PCN film, which were probably within the range of experimental errors or due to the presence of traces of DBP.

For typical nanoporous PCN-based films, the permittivity values ε' of PCN_{DMP30} and PCN_{DMP50} samples were respectively equal to 3.20 and 3.13 (at 1 kHz, Figure 7, curves 3 and 4). These values were a little bit lower than the value of permittivity for the neat PCN, thus indicating an existence of pores in the films, but in relatively small content. Such results were in accordance with the formation of nano-scale size pores associated with relatively low values of total pore volume in the PCN-based samples, as shown above by DSC-based thermoporometry (see Table 1).

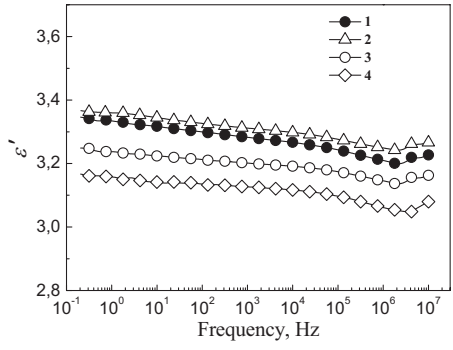

Figure 7.
Frequency dependence of permittivity (ε') for the samples studied: (1) neat PCN; (2) PCN_{DBP30}; (3) PCN_{DMP30}; (4) PCN_{DMP50}. All the samples were tested after annealing at $T = 250\,^{\circ}C$ for 2 h.

By using the mixing rules ($\log \varepsilon' = x \cdot \log \varepsilon'_1 + (1\text{-}x) \cdot \log \varepsilon'_2$ with x the pore content, ε'_1 and ε'_2 the dielectric constants of air (pores) and matrix, respectively), it was possible to assess that nanoporous PCN-based matrices contained about 5% of pores only, thus corresponding to a slight decrease in the effective permittivity of the medium. One can consider that some pores collapsed after annealing of the samples at $T = 250\,^{\circ}C$ for 2 h.

Finally, it could be concluded that the nanoporous films studied exhibited dielectric properties typical for PCN matrices with low pore contents.

Conclusion

Nanoporous films based on thermostable densely crosslinked PCN networks were generated using chemically-induced phase separation during the *in-situ* polycyclotrimerization of 4,4′-ethylidenediphenyl dicyanate in the presence of 20–50 wt.% of inert high-boiling temperature phthalates, *i.e.* DOP, DBP or DMP as porogens, followed by their extraction from the PCN frameworks, drying, and additional annealing at various temperatures to reach complete removal of non-extracted porogens. A catalytic metal complex, *i.e.* a mixture of cobalt acetyl acetonate with nonylphenol, was used to accelerate the reaction of polycyclotrimerization and to shift the reaction temperature interval to lower temperatures, as well as to minimize the dilution effect of liquid phthalates during the creation the film-forming materials. According to TGA data, all nanoporous PCN-based films studied could be considered as highly thermostable materials. The nanoporous structure for all PCN-based films developed was confirmed by SEM and DSC-based thermoporometry. The average

pore diameters and pore volume values were found in the range of 23–65 nm and 0.11–0.35 cm^3g^{-1}, respectively, depending on the porogen and the annealing temperature used, the pore diameters smaller than 50 nm representing up to ~80–90% of all the pore sizes. It is noteworthy that increasing phthalate contents and annealing temperatures were generally associated with larger pore diameters and higher pore volumes. Interestingly, the samples with higher pore volumes were characterized by the lower dielectric constants, as expected.

Nanoporous polycyanurate films possessing high thermal stability and low permittivity are expected to be promising materials for advanced applications in many branches of industry, including microelectronics, airspace technology, and automotive industry.

Acknowledgements: The authors gratefully acknowledge the NAS of Ukraine and the CNRS of France for financial support through PICS project No. 5700 (Ukraine-France cooperation 2011-2013).

[1] "*Chemistry and Technology of Cyanate Ester Resins*", I. Hamerton, Ed., Chapman & Hall, Glasgow **1994**.
[2] C. P. R. Nair, D. Mathew, K. N. Ninan, *Adv. Polym. Sci.* **2001**, *155*, 1.
[3] "Thermostable polycyanurates. Synthesis, modification, structure and properties", A. Fainleib, Ed., Nova Science Publishers, New York **2010**.
[4] "*Handbook of Membrane Separations Chemical, Pharmaceutical, Food, and Biotechnological Applications*", A. K., Pabby, S. S. H., Rizvi, A. M. Sastre, Eds., Taylor & Francis Group, **2009**.
[5] Y. Li, G. He, S. Wang, S. Yu, F. Pan, H. Wu, Z. Jiang, *J. Mater. Chem. A* **2013**, *1*, 10058.
[6] K.-S. Chang, K.-L. Tung, Y.-F. Lin, H.-Y. Lin, *RSC Adv.* **2013**, *3*, 10403.
[7] K. Gusakova, O. Grigoryeva, . Starostenko, A. Fainleib, D. Grande, "*Advances in progressive thermoplastic and thermosetting polymers: perspectives and applications*", E. Mamunya, M. Iurzhenko, Eds., TechnoPress, **2012**, chap. *6*, pp. 219–258.
[8] D. Grande, O. Grigoryeva, A. Fainleib, K. Gusakova, C. Lorthioir, *Eur. Polym. J.* **2008**, *44*, 3588.
[9] O. Grigoryeva, A. Fainleib, K. Gusakova, D. Grande, *Eur. Polym. J.* **2011**, *47*, 1736.
[10] D. Grande, O. Grigoryeva, K. Gusakova, A. Fainleib, *Eur. Polym. J.* **2013**, *49*, 2162.
[11] K. Gusakova, O. Starostenko, O. Grigoryeva, A. Fainleib, B. Youssef, J.-M. Saiter, G. Boiteux, D. Grande, *Polym. Mater. Sci. Eng.* **2013**, *108*, 34.
[12] I. Harismendy, C. M. Gómez, M. D. Río, I. Mondragon, *Polym. Int.* **2000**, *49*, 735.
[13] C. M. Gómez, I. B. Recalde, I. Mondragon, *Eur. Polym. J.* **2005**, *41*, 2734.
[14] M. Brun, A. Lallemand, J.-F. Quinson, C. Eyraud, *Thermochim. Acta* **1977**, *21*, 59.
[15] M. Iza, S. Woerly, C. Danumah, S. Kaliaguine, M. Bousmina, *Polymer* **2000**, *41*, 5885.
[16] J. L. Hedrick, T. P. Russell, J. C. Hedrick, J. G. Hilborn, *J. Polym. Sci., Part A: Polym. Chem.* **1996**, *34*, 2879.
[17] E. A. Grulke, "*Polymer Handbook. 3rd edition*", J. Brandrup, E. H. Immergut, Eds., Wiley, New York **1989**, pp. VII/ 519–559.
[18] "*Properties of Polymers*", D. W. Van Krevelen, Elsevier, Amsterdam **1990**.
[19] V. V. Korshak, P. N. Gribkova, A. V. Dmitrenko, A. G. Puchin, V. A. Pankratov, S. V. Vinogradova, *Vysokomol. Soed. A* **1974**, *16*, 15.
[20] M. L. Ramirez, R. Walters, R. E. Lyon, E. P. Savitski, *Polym. Degrad. Stab.* **2002**, *78*, 73.
[21] "*Handbook of Plasticizers, 2nd Edition*", G. Wypych, (Ed., **2012**, p. 748.
[22] S. Brunauer, P. Emmett, E. Teller, *J. Am. Chem. Soc.* **1938**, *60*, 309.
[23] Broadband Dielectric Spectroscopy. Ed., F. Kremer, A. Schönhals, Springer, Germany **2003**.

